Statistical mechanics of dense ionized matter. III. Dynamical properties of the classical one-component plasma

J.-P. Hansen
Laboratoire de Théorie des Liquides, Université de Paris VI, 4 Place Jussieu, Paris, France*

I. R. McDonald
Department of Chemistry, Royal Holloway College, Egham, Surrey, England

E. L. Pollock†
Department of Physics and Materials Research Laboratory, University of Illinois, Urbana, Illinois 61801
(Received 14 October 1974)

We present extensive molecular-dynamics (MD) computations of the time-dependent correlation functions of the classical one-component plasma over a wide range of thermodynamic states characterized by the dimensionless parameter $\Gamma = e^2/a\,k_B T$, where a is the ion-sphere radius. The computed velocity autocorrelation functions exhibit marked oscillations for $\Gamma \gtrsim 10$ at a frequency close to the plasma frequency, showing the existence of strong coupling between single-particle and collective modes; this is confirmed by a standard memory-function analysis. The dynamical structure factor consists of very sharp peaks near the plasma frequency, up to wave vectors of order $1/a$. The resulting dispersion curve exhibits negative dispersion for $\Gamma \gtrsim 3$. A simple memory-function analysis reproduces the MD data very well. At $\Gamma = 152.4$ our computations also provide evidence of well-defined shear modes. For large wave vectors a second, high-frequency transverse mode appears. From the correlation functions we have finally extracted estimates of the diffusion constant and the coefficient of shear viscosity. Near crystallization the shear viscosity has a value which is unusually large compared with that of simple liquids near the triple point.

I. INTRODUCTION

The first two papers[1,2] of this series (to be referred to as I and II) were devoted to the study of the equilibrium properties of the fluid and crystalline phases of the classical one-component plasma (OCP) by the Monte Carlo method of Metropolis *et al.*[3] In the present paper we describe the results of a series of molecular-dynamics (MD) "experiments" on the dynamical properties of the OCP and show how they may be interpreted in the framework of generalized hydrodynamics. Some parts of the work have been briefly reported elsewhere,[4] in a Note to be referred to as III.

The algorithm of Verlet[5] was used to integrate numerically the classical equations of motion of a system of 250 ions, each with mass m and charge Ze, contained within a periodically repeating cube. As the unit of length we choose the ion-sphere radius a (note that in II the ion-sphere radius is denoted by the sumbol $\bar{r}$), defined as

$$a = (3/4\pi\rho)^{1/3},$$

where ρ is the number density, and as the unit of time we choose the inverse plasma frequency ω_p^{-1}, where

$$\omega_p^2 = 4\pi\rho(Ze)^2/m.$$

The forces were calculated by an Ewald method[6] in order to account for the long range of the Coulombic interaction; the uniform background, which is assumed to be stationary, has no effect on the dynamics of the ions.

We recall that the configurational thermodynamic properties of the OCP are determined by the dimensionless parameter Γ, given by

$$\Gamma = (Ze)^2/ak_BT,$$

and that the Monte Carlo work described in earlier papers of the series has shown that the OCP crystallizes at $\Gamma = 155 \pm 10$. The results reported here are based on a series of MD runs at six values of Γ. Some technical details of the calculations (length and number of the time steps in the numerical integrations) are given in Table I. The values quoted for Γ are time averages over the run; the largest Γ value is located very near the melting transition.

The outline of the paper is as follows. In Sec. II we discuss the self-motion of the ions. Sections III and IV are devoted to an analysis of results on the dynamical structure factor and Sec. V to an interpretation of data on the transverse currents. Finally, in Sec. VI we summarize briefly the results we have obtained and give numerical values for the computed transport coefficients.

TABLE I. Time increments Δt (in units of ω_P^{-1}) and total number of time steps N_t for each of the six MD runs.

Γ	0.993	9.7	19.7	59.1	110.4	152.4
Δt	0.02	0.03	0.05	0.1	0.1	0.1
N_t	10^5	3×10^3	10^3	12×10^3	5×10^4	10^5

II. VELOCITY AUTOCORRELATION FUNCTION AND SELF-DIFFUSION COEFFICIENT

The self-motion of the ions may be studied via a calculation of the (normalized) velocity autocorrelation function $Z(t)$, defined as

$$Z(t)=\langle \vec{v}_i(t')\vec{v}_i(t'+t)\rangle/\langle \vec{v}_i(t')^2\rangle . \tag{2.1}$$

The angular brackets denote a double average over, first, the 250 ions labeled i and, second, all choices of the time origin t'. The results obtained for $Z(t)$ at various values of Γ are displayed in Fig. 1. We see that for $\Gamma=0.993$ the autocorrelation falls monotonically to zero, but at larger Γ the decay is characterized by the appearance at large times of oscillations at a frequency close to ω_p. The oscillations are already evident at $\Gamma=9.7$ and become more pronounced as Γ increases. The onset of these oscillations is an indication of the fact that at sufficiently high charge densities the motion of *single* ions is strongly coupled to the *collective* density fluctuations, or "plasmon" modes, which are discussed in greater detail in Secs. II and III.

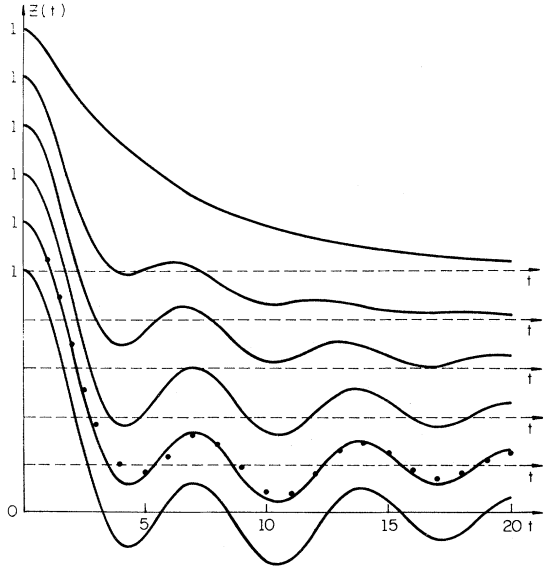

FIG. 1. Normalized velocity autocorrelation function for (reading from top to bottom) $\Gamma=0.993$, 9.7, 19.7, 59.1, 110.4, and 152.4. The time scale is in units of ω_p^{-1}. The points for $\Gamma=110.4$ show the results of the memory-function fit, Eqs. (2.9) and (2.10). Note the extension of the time scale in the case of $\Gamma=0.993$.

The computed power spectra $\tilde{Z}(\omega)/\tilde{Z}(0)$, where $\tilde{Z}(\omega)$ is the Fourier-Laplace transform of $Z(t)$, are plotted in Fig. 2. Inspection of these curves confirms the remark made in the previous paragraph; a persisting feature is the pronounced peak near the plasma frequency. At large values of Γ there is also a diffusive peak at a nonzero frequency which resembles that observed in uncharged liquids at high densities. At $\Gamma=110.4$ a shoulder appears on the diffusive peak which develops into a prominent wing as Γ decreases; simultaneously, the low-frequency peak disappears. Thus over a wide range of Γ the structure of $\tilde{Z}(\omega)$ corresponds to a broad diffusive background with a superimposed "plasmon"-type peak which disappears only for $\Gamma\approx1$. The position ω_{max} of the high-frequency peak is remarkably constant, occurring everywhere at $\omega_{max}/\omega_p=0.91\pm0.02$.

In order to gain some insight into the character of the processes regulating the self-motion it is useful to analyze the results on the velocity autocorrelation through the well-known memory-function formalism. We proceed by writing the rate of decay of $Z(t)$

$$\dot{Z}(t)=-\int_0^t M(s)Z(t-s)\,ds, \tag{2.2}$$

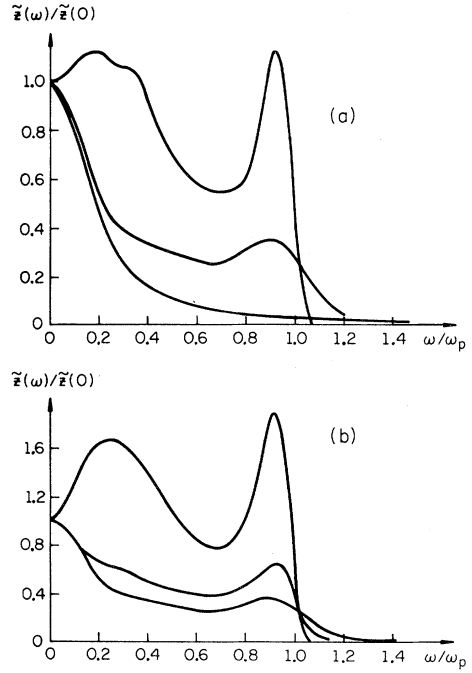

FIG. 2. Normalized power spectrum of the velocity autocorrelation function as a function of ω/ω_p for (reading from top to bottom) $\Gamma=110.4$, 19.7, and 0.993 in (a) and $\Gamma=152.4$, 59.1, and 9.7 in (b).

where $M(t)$ is the memory function for the autocorrelation $Z(t)$. An advantage of making the analysis in terms of the memory function rather than of the velocity autocorrelation itself is the possibility it offers of differentiating relatively clearly between the short-time relaxation processes and the effects, dominant at large times, which arise from the coupling between the pure diffusive mode and the collective modes of the system. This possibility has already been fruitfully exploited by Levesque and Verlet[7] in their study of diffusion in the Lennard-Jones fluid. In the present case such an approach is likely to be most useful at large Γ values, where the time scales of the two different processes do not greatly overlap (cf. Fig. 2).

To analyze the short-time behavior we begin by expanding the self-intermediate-scattering-function $F_s(q,t)$ as a Taylor series in powers of t,

$$F_s(q,t)=1-\omega_{0s}^2\frac{t^2}{2!}+\omega_{0s}^2\omega_{1s}^2\frac{t^4}{4!}-\omega_{0s}^2\omega_{2s}^4\frac{t^6}{6!}+\cdots, \tag{2.3}$$

where q is a wave vector in units of a^{-1}. On applying the equations of motion, we find, choosing ω_p^{-1} as the unit of time, that

$$\begin{aligned}\omega_{0s}^2&=q^2/3\Gamma,\\ \omega_{1s}^2&=\tfrac{1}{3}+q^2/\Gamma,\\ \omega_{2s}^4&=\tfrac{1}{9}[(12J+1)+15q^2/\Gamma+15q^4/\Gamma^2],\end{aligned} \tag{2.4}$$

where

$$J=\int_0^\infty r^{-4}g(r)\,dr. \tag{2.5}$$

It is known from earlier Monte Carlo work on the OCP that J can be fitted for all values of Γ by

$$J=a_0+\frac{a_1}{\Gamma^{1/2}}+\frac{a_2}{\Gamma}+\frac{a_3}{\Gamma^{3/2}}+\frac{a_4}{\Gamma^2}+\frac{a_5}{\Gamma^3}, \tag{2.6}$$

with

$$\begin{aligned}a_0&=0.135\,729\,02, & a_1&=0.173\,617\,18,\\ a_2&=0.927\,066\,05, & a_3&=-0.097\,396\,74,\\ a_4&=1.782\,425\,3, & a_5&=1.987\,851.\end{aligned}$$

The normalized velocity autocorrelation is given by

$$Z(t)=\lim_{q\to 0}\left(-\frac{1}{\omega_{0s}^2}\frac{\partial^2 F_s(q,t)}{\partial t^2}\right). \tag{2.7}$$

The short-time expansion of $Z(t)$ is therefore

$$Z(t)=1-\frac{1}{3}\frac{t^2}{2!}+\frac{12J+1}{9}\frac{t^4}{4!}-\cdots. \tag{2.8}$$

The function $M(t)$ also has a Taylor-series expansion in powers of t^2. The coefficient of t^{2n} in the expansion of $M(t)$ is determined by the first $n+1$ even moments of $Z(t)$. If we adopt the more or less standard procedure of choosing a Gaussian form for $M(t)$ to represent the short-time relaxation we may incorporate the first three nonvanishing moments of $Z(t)$ exactly by writing

$$M(t)=\tfrac{1}{3}e^{-2Jt^2}. \tag{2.9}$$

Some results on the "exact" memory functions obtained by solving Eq. (2.2) for $M(t)$ with the molecular-dynamics data on $Z(t)$ are shown in Fig. 3. The curves are more strongly damped than those of the autocorrelation functions. The dominant feature, except at the smallest Γ, is the long-time tail which oscillates about zero with a period of approximately 2π. Clearly it is this tail which is responsible [in the context of Eq. (2.2)] for the "plasmon"-type oscillations in $Z(t)$. In order to describe the asymptotic behavior quantitatively, we have fitted $M(t)$ for $t\gtrsim 2\pi$ through the function

$$M(t)\sim At^3\sin[(1+\Delta)t]e^{-t/\tau}, \tag{2.10}$$

where A measures the strength and τ the lifetime of the long-time tail, Δ is a small phase factor, and the unit of time is again ω_p^{-1}.

By combining Eqs. (2.9) and (2.10), we obtain a fair fit to the computer-generated $Z(t)$ at large Γ, as shown by the results for $\Gamma=110.4$, which are plotted in Fig. 1. In reality, however, the situation is considerably more complicated. At lower

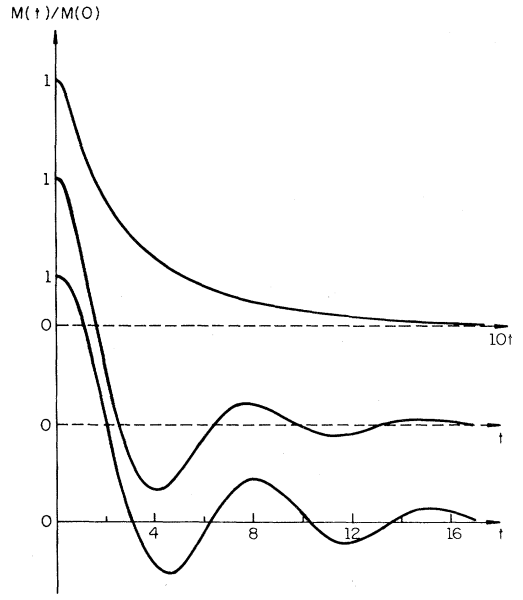

FIG. 3. "Exact" memory function of the velocity autocorrelation function for (reading from top to bottom) $\Gamma=0.993$, 19.7, and 110.4. The time scale is in units of ω_p^{-1}.

values of Γ the time scale of the two processes involved are not so clearly separable, and a simple superposition of the short- and long-time approximations to $M(t)$, Eqs. (2.9) and (2.10), is not successful. Furthermore, even at short times, the Gaussian approximation (2.9) is not very accurate. This fact is very obvious at $\Gamma = 0.993$, but even at higher values of Eq. (2.9) it predicts too rapid a decay of $M(t)$. Knowledge of the sixth moment of $Z(t)$ would allow the use of a more flexible form of short- and intermediate-time approximations, but it is obvious that the task of parameterizing $Z(t)$ fully is a very difficult task. We have therefore not pursued the matter further.

Finally, we have evaluated the dimensionless self-diffusion coefficient $D^* = D/\omega_p a^2$ from the infinite-time integral of $Z(t)$,

$$D^* = \frac{1}{3\Gamma}\int_0^\infty Z(t)\,dt. \tag{2.11}$$

The results are listed in Table II, from which we see that the striking changes which occur in $Z(t)$ as Γ increases are accompanied by a correspondingly rapid variation in D^*. A log-log plot of D^* as a function of Γ is approximately linear, and D^* is everywhere fitted within 20%, except at the lowest Γ value, by the simple formula

$$D^* = C\Gamma^{-a}, \tag{2.12}$$

with $C = 2.95$ and $a = 1.34$. It should be noted that at large values of Γ (~100) the collective oscillations in the tail of $Z(t)$ make very little contribution to D, and the short-time approximation (2.9) accounts for the larger part of the value calculated from Eq. (2.12).

III. LONGITUDINAL COLLECTIVE MODES: THE DISPERSION RELATION

In theoretical treatments of the collective modes of many-particle systems it is customary to discuss the problem in terms of, first, the density operator

$$\rho_{\vec{k}}(t) = \sum_{i=1}^{N} e^{i\vec{k}\cdot\vec{r}_i(t)} \tag{3.1}$$

and, second, the current operator

$$\vec{j}_{\vec{k}}(t) = \sum_{i=1}^{N} \vec{v}_i(t) e^{i\vec{k}\cdot\vec{r}_i(t)}, \tag{3.2}$$

TABLE II. Reduced diffusion constant D^* as a function of Γ.

Γ	0.993	9.7	19.7	59.1	110.4	152.4
D^*	2.01	0.130	0.060	0.015	0.0051	0.0032

where $\vec{r}_i$ $(i = 1, \ldots, N)$ are the position vectors of the particles and $\vec{v}_i$ are the particle velocities. The time evolution of these quantities is described by their correlation functions. The density-density correlation function, generally referred to as the intermediate scattering function, is defined by

$$F(k, t) = (1/N)\langle \rho_{\vec{k}}(t)\,\rho_{-\vec{k}}(0)\rangle, \tag{3.3}$$

where the brackets denote a statistical average. The Fourier transform of this function is the familiar dynamical structure factor

$$S(k, \omega) = \frac{1}{2\pi}\int_{-\infty}^{+\infty} e^{i\omega t} F(k, t)\,dt, \tag{3.4}$$

which is simply the spectrum of the density fluctuations of the system. It should be noted that in the case of the OCP $S(k, \omega)$ is also the spectrum of the *charge* fluctuations, which coincide with the density fluctuations because of the rigidity of the uniform background.

The current (3.2) may be separated into its components parallel and perpendicular to the wave vector $\vec{k}$, and, correspondingly, we may consider two separate correlation functions, the longitudinal-current correlation function, defined by

$$C_l(k, t) = (1/N)\langle \vec{k}\cdot\vec{j}_{\vec{k}}(t)\vec{k}\cdot\vec{j}_{-\vec{k}}(0)\rangle, \tag{3.5}$$

and the transverse-current correlation function

$$C_t(k, t) = (1/2N)\,\mathrm{Tr}\langle(\vec{k}\times\vec{j}_{\vec{k}}(t))(\vec{k}\times\vec{j}_{-\vec{k}}(0))\rangle. \tag{3.6}$$

On choosing $\vec{k}$ along the z axis, (3.5) and (3.6) reduce to

$$C_l(k, t) = \frac{k^2}{N}\left\langle \sum_{i=1}^{N} v_i^z(t) e^{ikz_i(t)} \sum_{j=1}^{N} v_j^z(0) e^{-ikz_j(0)} \right\rangle,$$

$$C_t(k, t) = \frac{k^2}{N}\left\langle \sum_{i=1}^{N} v_i^x(t) e^{ikz_i(t)} \sum_{j=1}^{N} v_j^x(0) e^{-ikz_j(0)} \right\rangle.$$

The study of the transverse (or "shear") mode is postponed until Sec. V; here we shall deal only with the longitudinal currents.

We first introduce the Fourier-Laplace transform of (3.5),

$$\tilde{C}_l(k, \omega) = \int_0^\infty e^{i\omega t} C_l(k, t)\,dt. \tag{3.7}$$

Integrating (3.4) twice by parts yields immediately the well-known relation

$$S(k, \omega) = (1/\pi\omega^2)\tilde{C}_l'(k, \omega), \tag{3.8}$$

where the prime denotes the real part. $S(k, \omega)$ is also related to the density response function

$$\chi(k, \omega) = \frac{1}{N}\int_0^\infty e^{i\omega t}\langle\{\rho_{\vec{k}}(t), \rho_{-\vec{k}}(0)\}\rangle\,dt, \tag{3.9}$$

where $\{\ \}$ denotes the Poisson bracket, by

$$S(k,\omega) = -(1/\pi\beta\rho\omega)\,\chi''(k,\omega), \tag{3.10}$$

where the double prime denotes the imaginary part. This last relation will be used in Sec. III, where we analyze the computer data on the basis of a standard phenomenological theory.

We now replace the vector $\vec{k}$ by the dimensionless vector $\vec{q} = a\vec{k}$. The three lowest-order sum rules obeyed by $S(q,\omega)$ are

$$\langle\omega^0\rangle = \int_{-\infty}^{+\infty} S(q,\omega)\,d\omega = S(q), \tag{3.11}$$

$$\langle\omega^2\rangle = \int_{-\infty}^{+\infty} \omega^2 S(q,\omega)\,d\omega = \frac{\omega_p^2 q^2}{3\Gamma} = \omega_0^2, \tag{3.12}$$

$$\langle\omega^4\rangle = \int_{-\infty}^{+\infty} \omega^4 S(q,\omega)\,d\omega = \frac{\omega_p^4}{3\Gamma}\left(\frac{q^4}{\Gamma} + q^2 - 2q^2 I(q)\right), \tag{3.13}$$

where $S(q)$ is the structure factor and

$$I(q) = \int_0^\infty \frac{1}{r}\,[g(r)-1] \times\left(\frac{\sin qr}{qr} + \frac{3\cos qr}{q^2r^2} - \frac{3\sin qr}{q^3r^3}\right)dr.$$

Here r is expressed in units of a and $g(r)$ is the radial distribution function. It should be noted that (3.13) differs from the usual fourth-moment sum rule[8] by an additional term stemming from the uniform background.

We have computed $S(q,\omega)$ numerically by calculating the time average

$$S(q,\omega) = \frac{1}{2\pi N}\int_{-\infty}^{+\infty} e^{i\omega t}\,\langle\rho_{\vec{q}}(t)\,\rho_{-\vec{q}}(0)\rangle\,dt$$
$$= \frac{1}{2\pi N}\lim_{T\to\infty}\frac{1}{T}\int_0^T e^{i\omega t}\,\rho_{\vec{q}}(t)\,dt \times\int_0^T e^{-i\omega t'}\rho_{-\vec{q}}(t')\,dt'$$
$$= \frac{1}{2\pi N}\lim_{T\to\infty}\frac{1}{T}\,|\rho_{\vec{q}}(\omega)|^2, \tag{3.14}$$

where $\rho_{\vec{q}}(\omega)$ is the Fourier-Laplace transform of the density operator (3.1). Calculations were made at $\Gamma = 0.993$, 9.7, 110.4, and 152.4. As we have remarked earlier, the last value is close to crystallization.[2] For each state the calculations cover seven values of the wave number q, including the smallest q value compatible with the size of the system, i.e., $2\pi a/L$, equal to 0.619 for our 250-particle system. The most striking result of the computations is the appearance at the three largest Γ values of very sharp peaks in $S(q,\omega)$ for wave numbers up to $q \approx 2$. At $\Gamma = 0.993$ the peaks are considerably broader, and in all cases they broaden rapidly as q increases. The numerical results for four wave vectors are shown in Figs. 4–7, and the peak positions $\omega(q)$ and linewidths are shown in Fig. 8. From the latter it is immediately clear that for $\Gamma = 0.993$ the dispersion is *positive*, in agreement with the predictions of simple Vlasov or mean-field theory,[9] whereas for the larger Γ values the dispersion is always *negative*. In the limit $q \to 0$ we find that $\omega(q) \to \omega_p$, as is to be ex-

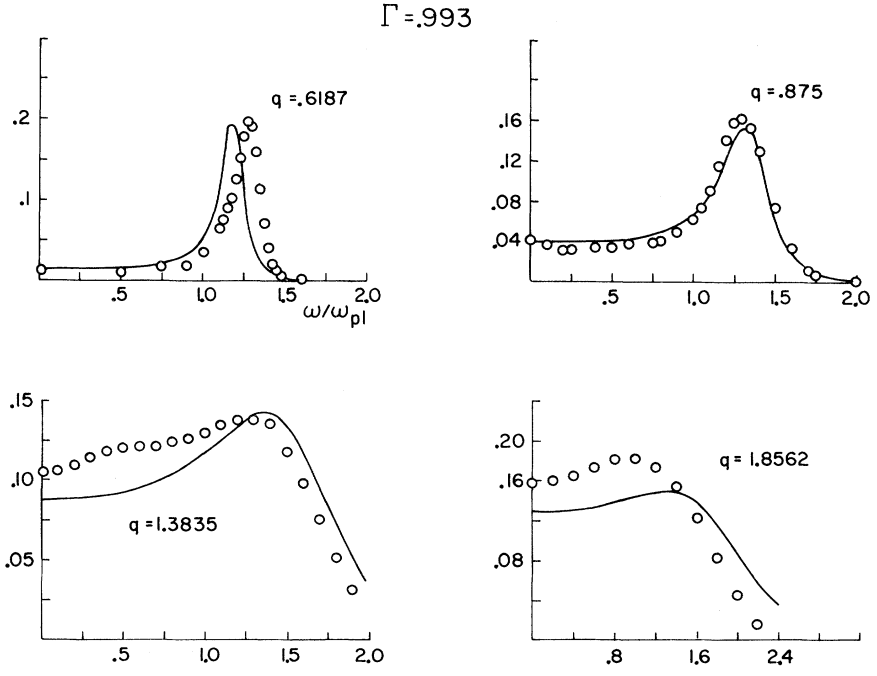

FIG. 4. $S(q,\omega)$ as a function of ω/ω_p, from the MD calculations (circles) and from the memory function fit, Eq. (4.8) (solid line), $\Gamma = 0.993$, and indicated q values. The MD results have been normalized to the $S(q)_{M.C.}$ values listed in Table III.

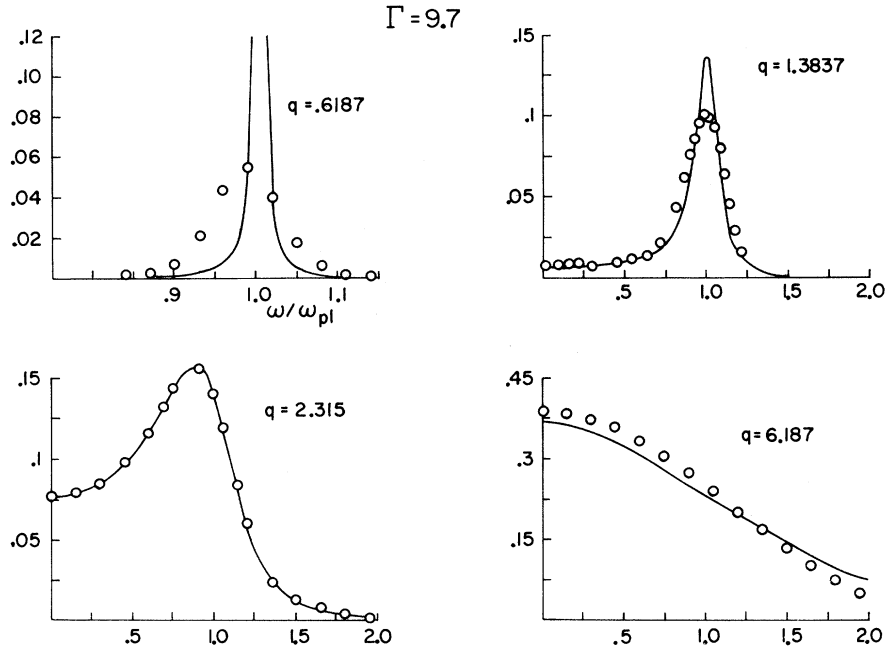

FIG. 5. Same as Fig. 4, but for $\Gamma = 9.7$. Note that the x axis for $q = 0.6187$ does not start at the origin.

pected.

In III the behavior of $\omega(q)$ was analyzed with the help of a Gaussian representation of $S(q, \omega)$ and the moment sum rules (3.11)–(3.13). We repeat the analysis here in an even simpler form. As $q \to 0$, $S(q, \omega)$ reduces to a sum of δ functions $[\delta(\omega - \omega_p) + \delta(\omega + \omega_p)]$ (cf. Appendix B). For small q our computations show that $S(q, \omega)$ is still very sharp; so we use a simple zero-width (i.e., infinite-lifetime) representation,

$$S(q, \omega) = A(q)[\delta(\omega - \omega(q)) + \delta(\omega + \omega(q))]. \qquad (3.15)$$

$A(q)$ and $\omega(q)$ may be determined from the sum rules (3.11) and (3.12), giving

$$A(q) = \tfrac{1}{2}S(q), \quad \omega^2(q) = (\omega_p^2/3\Gamma)q^2/S(q), \qquad (3.16)$$

which is reminiscent of the Feynman expression for the excitation spectrum of liquid helium.[10]

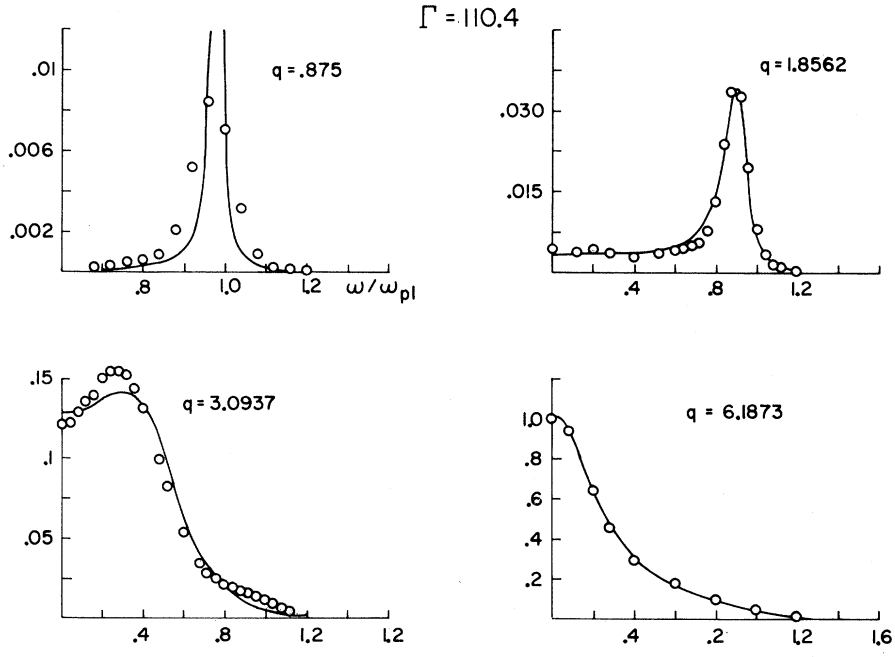

FIG. 6. Same as Fig. 4, but for $\Gamma = 110.4$.

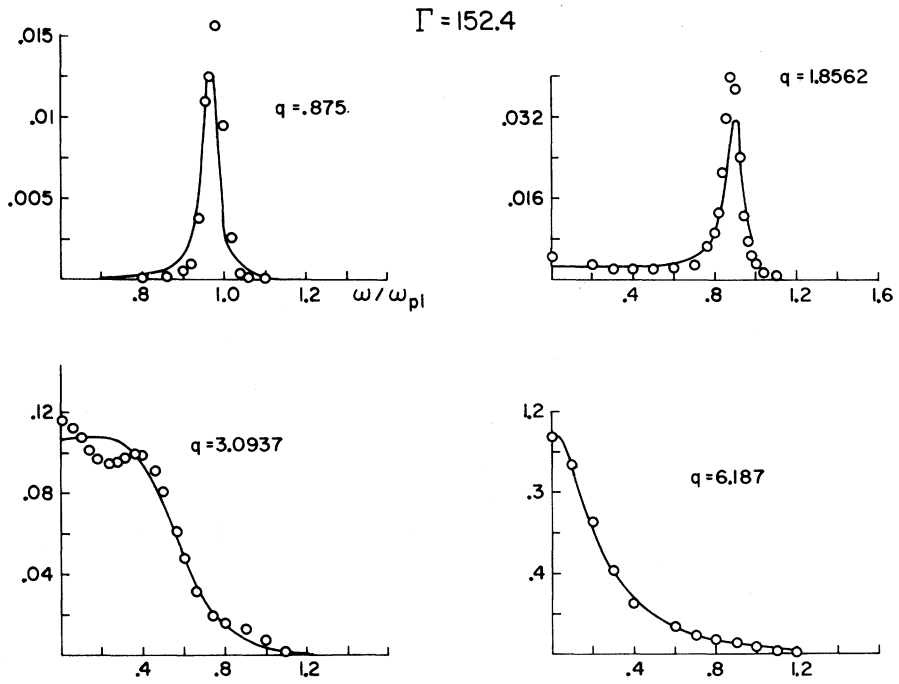

FIG. 7. Same as Fig. 4, but for $\Gamma=152.4$.

In order to study the small-q behavior of (3.16), we write $S(q)$, to order q^4, in the form

$$S(q) = (q^2/3\Gamma)(1+\delta q^2). \tag{3.17}$$

The first term gives the exact behavior as $q \to 0$.[11] The coefficient δ of the first correction term can be determined empirically from the computer results or, for $\Gamma \lesssim 10$, from the HNC results.[12] δ can also be expressed as the fourth "moment" of $g(r)$, i.e.,

$$\delta = \frac{\Gamma}{40}\int_0^\infty r^4[g(r)-1]r^2\,dr. \tag{3.18}$$

Empirically it turns out that δ is negative for $\Gamma \lesssim 3$ and positive at higher Γ. This change seems to coincide with the onset of oscillations in $g(r)$. Substituting (3.1) into (3.16) yields the dispersion relation to order q^2,

$$\omega^2(q) = \omega_p^2(1-\delta q^2). \tag{3.19}$$

This is a generalization of the well-known Vlasov dispersion relation[9]

$$\omega^2(q) = \omega_p^2(1+q^2/\Gamma). \tag{3.20}$$

Equation (3.19) predicts a change from positive to negative dispersion at the value of Γ where δ changes sign, i.e., $\Gamma \approx 3$; it must be stressed, however, that (3.19) is only valid to order q^2. The coefficient δ increases with Γ and hence (3.19) predicts stronger negative dispersion with increasing Γ, in agreement with our findings summarized in Fig. 8. The possibility of negative dispersion has been independent proposed by Abramo and Tosi.[13]

IV. PHENOMENOLOGICAL ANALYSIS OF THE DYNAMICAL STRUCTURE FACTOR

It is apparent from Figs. 4–7 that the form of $S(q,\omega)$ changes considerably over the range of q values covered by our computations. At the smallest q it reduces to a well-defined peak which broadens as Γ decreases, while at a q value 10 times larger, corresponding roughly to the inverse of the average interparticle distance, $S(q,\omega)$ is already very near its ideal-gas limit $S_0(q,\omega)$, given by

$$S_0(q,\omega) = (3\Gamma/2\pi)^{1/2}(1/q)e^{-3\Gamma\omega^2/2q^2}, \tag{4.1}$$

where ω is expressed in units of ω_p.

We shall now investigate the extent to which the rapidly varying character of $S(q,\omega)$ can be accounted for on the basis of existing theoretical approaches.

We first consider a number of theories of the mean-field type. The best-known examples of such theories are those based on the Vlasov kinetic equation or on the equivalent random-phase approximation (RPA). In these approximations $S(q,\omega)$ takes the form[14]

$$S^{\mathrm{MF}}(q,\omega) = \frac{S_0(q,\omega)}{[1-\tilde{v}(q)\phi(z)]^2+[\omega\pi\tilde{v}(q)S_0(q,\omega)]^2}, \tag{4.2}$$

where MF stands for "mean field";

$$v(q) = 3\Gamma/q^2$$

is the Fourier transform of the Coulomb potential, divided by $k_B T$, $z = (\frac{3}{2}\Gamma)^{1/2}\omega/q$, and

$$\phi(z) = -[1 - 2zF(z)],$$

where

$$F(z) = e^{-z^2}\int_0^z e^{t^2}\,dt$$

is Dawson's integral. For details of the derivation of Eq. (4.2) we refer the reader to a recent paper by Kugler.[14]

In Fig. 9 we compare the curves of $S^{\mathrm{MF}}(q,\omega)$ calculated from Eq. (4.2) at two values of the wave vector with the computer results obtained at $\Gamma = 0.993$. It can be seen that $S^{\mathrm{MF}}(q,\omega)$ is too sharp at the smaller q value and too broad at the larger. These defects become much worse at higher values of Γ, where the low-q $S^{\mathrm{MF}}(q,\omega)$ reduce practically to δ functions. This is obviously due to the complete neglect of "collisional damping" in the mean-field approximation.

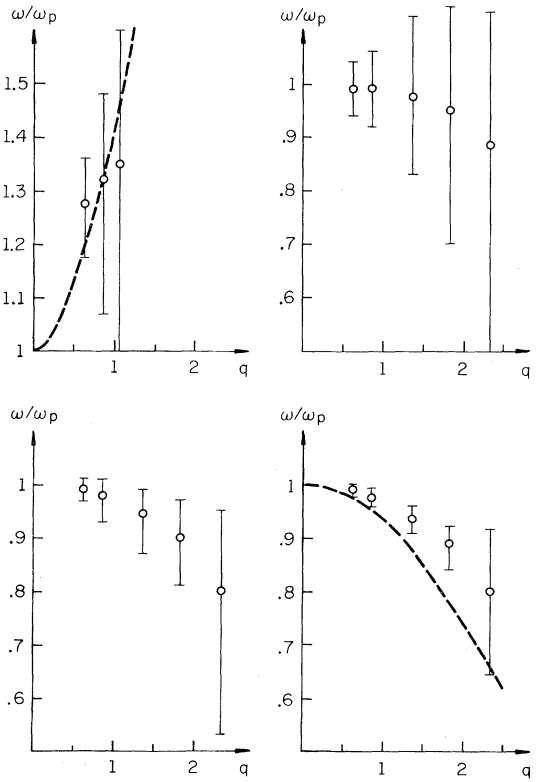

FIG. 8. Dispersion curves $\omega(q)/\omega_p$ as a function of q for the "plasmon" modes at $\Gamma = 0.993$, 9.7, 110.4, and 152.4. The vertical lines indicate widths at half-maximum value of $S(q,\omega)$; note the increasing asymmetry at the larger q values. The dashed curve at $\Gamma = 0.993$ corresponds to the Vlasov dispersion relation (3.20); the dashed curve at $\Gamma = 152.4$ corresponds to the quasi-harmonic Wigner lattice along the [100] direction (cf. II).

The mean-field theories can be improved by replacing $\tilde{v}(q)$ by the "effective potential"

$$\tilde{v}_{\mathrm{eff}}(q) = -\tilde{c}(q) = [1 - S(q)]/S(q),$$

where $\tilde{c}(q)$ is the Fourier transform of the Ornstein-Zernike direct correlation function $c(r)$.[15] The resulting $S(q,\omega)$ automatically satisfies the exact zeroth- and second-moment sum rules. This modification yields little improvement in the linewidth at low q, but the peak position is shifted, as the dispersion relation now becomes, to order q^2,

$$\omega^2(q) = \omega_p^2[1 - q^2(\delta - 2/3\Gamma)],$$

which reduces to the result of Eq. (3.19) in the limit of large Γ.

In a similar fashion, the second and fourth moments can be fitted exactly if one replaces $\tilde{v}(q)$ by another "effective potential"

$$\tilde{v}_{\mathrm{eff}}(q) = 3\Gamma/q^2 - 6\Gamma I(q)/q^2.$$

The improvement over the conventional mean-field approximation is again only marginal, confirming the complete failure of the mean-field picture to describe the dynamics of dense plasmas. It is clear that the situation can only be improved by taking into account the collisions between particles,

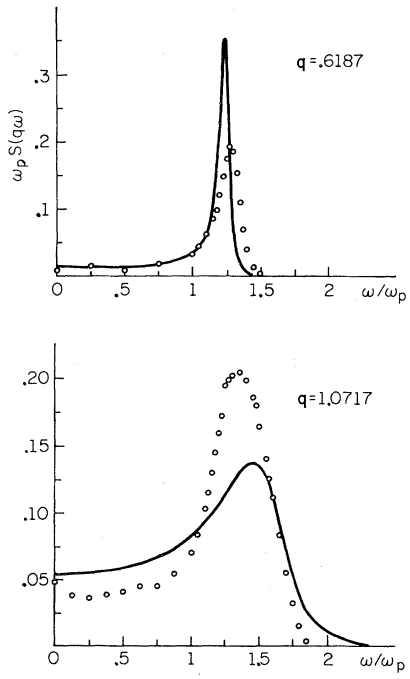

FIG. 9. Comparison between $S(q,\omega)$ calculated by MD (circles) and the mean-field approximation (4.2) (full lines) at $\Gamma = 0.993$ and for $q = 0.619$ and $q = 1.072$.

and calculations for the OCP which explicitly incorporate a collisional operator into the kinetic theory are presently under way.[16]

The second theoretical approach which we have investigated is based on the damping-function (or memory-function) formalism of Kadanoff and Martin.[17] The first step is to rewrite the response function (3.9) in terms of an unknown damping function $D(k,\omega)$,

$$\chi(k,\omega)=\frac{\rho k^2/m}{\omega^2-\Omega_0^2-i\omega k^2 D(k,\omega)}, \tag{4.3}$$

where

$$\Omega_0^2=k^2/\beta m S(k)=\omega_0^2/S(k).$$

A spectral representation for $D(k,\omega)$ is then introduced:

$$iD(k,\omega)=\int_{-\infty}^{+\infty}\frac{1}{\pi}\,\frac{D_1(k,\omega)}{\omega-\omega'+i\epsilon}\,d\omega'. \tag{4.4}$$

From the asymptotic expansion of $D(k,\omega)$ obtained from (4.4), one can write down an asymptotic expansion of $\chi(k,\omega)$ by using (4.3),

$$\chi(k,\omega)\sim\frac{\rho k^2}{m\omega^2}\left[1+\frac{\Omega_0^2+k^2\langle D_1\rangle}{\omega^2}+\frac{k^2\langle\omega'^2D_1\rangle+(k^2\langle D_1\rangle+\Omega_0^2)^2}{\omega^4}+O\left(\frac{1}{\omega^6}\right)\right], \tag{4.5}$$

with

$$\langle\omega'^{2n}D_1\rangle=\int_{-\infty}^{+\infty}\frac{1}{\pi}\,\omega'^{2n}D_1(k,\omega')\,d\omega'.$$

On the other hand, the response function and the dynamical structure factor are related by the standard formula of linear response theory,[18]

$$\chi(k,\omega)=\rho\beta\int_{-\infty}^{+\infty}\frac{S(k,\omega')}{\omega^2-(\omega'-i\epsilon)^2}\,d\omega',$$

from which we may derive the asymptotic expansion

$$\chi(k,\omega)\approx\frac{\rho\beta}{\omega^2}\left[\langle\omega'^2S\rangle+\frac{\langle\omega'^4S\rangle}{\omega^2}+\frac{\langle\omega'^6S\rangle}{\omega^4}+O\left(\frac{1}{\omega^6}\right)\right]. \tag{4.6}$$

Identification of (4.5) and (4.6) yields the moments of $D_1(k,\omega)$ as functions of the moments of $S(k,\omega)$:

$$\begin{aligned}&k^2\langle D_1\rangle=\langle\omega'^4S\rangle/\langle\omega'^2S\rangle-\Omega_0^2,\\&k^2\langle\omega'^2D_1\rangle=\langle\omega'^6S\rangle/\langle\omega'^2S\rangle-(\langle\omega'^4S\rangle/\langle\omega'^2S\rangle)^2.\end{aligned} \tag{4.7}$$

Through Eqs. (3.10) and (4.3), $S(k,\omega)$ can be expressed as a function of $D_1(k,\omega)$:

$$S(k,\omega)=\frac{(1/\pi)(k^2/\beta m)k^2D_1(k,\omega)}{[\omega^2-\Omega_0^2+k^2D''(k,\omega)]^2+[\omega k^2D_1(k,\omega)]^2}, \tag{4.8}$$

where $D''(k,\omega)$, the imaginary part of $D(k,\omega)$, must be calculated using (4.4).

An approximate parameterized form for $D_1(k,\omega)$ may now be assumed and the values of the parameters determined from (4.7). In the case of the Lennard-Jones liquid, a simple Gaussian form of $D_1(k,\omega)$ has proved very successful.[19] We have adopted the same form and write that

$$D_1(k,\omega)=C_1e^{-C_2\omega^2}, \tag{4.9}$$

where C_1 and C_2 are chosen such that $D_1(k,\omega)$ satisfies the first two moments conditions, (4.7),

$$\begin{aligned}&C_1=\langle D_1\rangle(\tfrac{1}{2}\pi\langle D_1\rangle/\langle\omega'^2D_1\rangle)^{1/2},\\&C_2=\langle D_1\rangle/2\langle\omega'^2D_1\rangle.\end{aligned} \tag{4.10}$$

This procedure ensures that $S(k,\omega)$ has the correct zeroth, second, fourth, and sixth moments.

The method we have outlined can be expected to be successful only when $D_1(k,\omega)$ has a single nonresonant form. In Fig. 10 we compare $D_1(k,\omega)$ extracted from the molecular-dynamics results at $\Gamma=0.993$ with the corresponding spectral function obtained from the Vlasov equation. It is seen that the actual $D_1(k,\omega)$ is much simpler than the Vlasov prediction. The additional "collisional damping" smoothes the peak predicted by the Vlasov equation and extends the function to higher frequencies. For this reason the simple Gaussian approximation, Eq. (4.9), can be expected to work moderately well, but might be less satisfactory at still smaller values of Γ.

To evaluate C_1 and C_2 we use as input data the zeroth, second, and fourth moments of $S(q,\omega)$, calculated from Eqs. (3.11)–(3.13), with the struc-

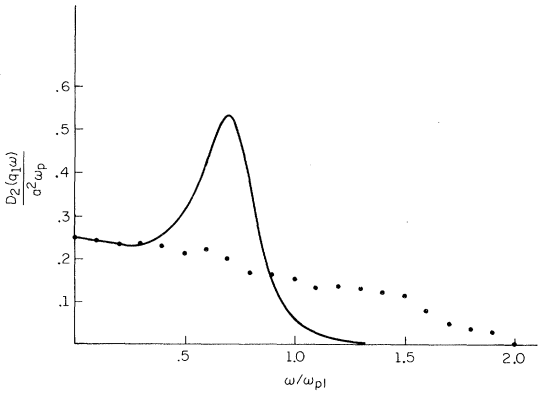

FIG. 10. Comparison of the dimensionless spectral function $D_1(q,\omega)/a^2\omega_p$ extracted from the MD data at $\Gamma=0.993$, $q=0.875$ (dots) with the corresponding function from mean-field theory (full line).

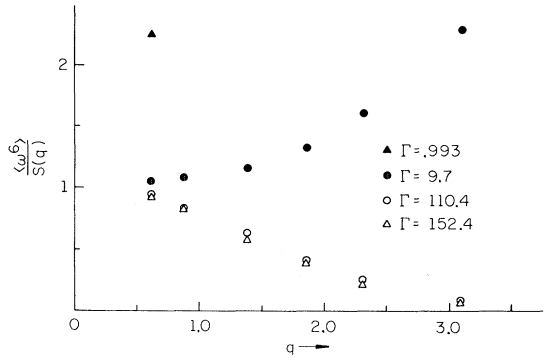

FIG. 11. Normalized sixth moment of $S(q,\omega)$, $\langle\omega^6\rangle/S(q)$, as obtained from the least-square fits of the MD data through Eq. (4.8), as a function of q, for $\Gamma=0.993$, 9.4, 110.4, and 152.4. The values of $S(q)$ used are listed in Table III.

ture factors and radial distribution functions obtained in I. The expression for the sixth moment, derived in the Appendix, involves the triplet correlation function; this moment has not yet been calculated "exactly" and we use it as a variable parameter to obtain a best least-squares fit to the MD data. The results for four q vectors at each of the four Γ values for which we have evaluated $S(q,\omega)$ are shown in Figs. 4–7. The agreement with the MD results is good. In particular the theoretical curves reproduce rather well the rapid variation in shape of the dynamical structure factor over a small range of q values, from a single sharp peak centered around ω_p to a broad line typical of single-particle behavior.

The fits are least satisfactory at low q partly because the sharply peaked $S(q,\omega)$ causes the moments to all be roughly equal to $S(q)$. Hence small errors in $\langle\omega^0\rangle$ and $\langle\omega^4\rangle$ cause larger errors in the moments of D_1 [Eq. (4.7)] and thus in the fitting parameters C_1 and C_2. In Fig. 11 the optimum values of $\langle\omega'^6S\rangle/S(q)$ are plotted versus q. The $S(q)$ and $I(q)$ [Eq. (3.13)] used to compute $\langle\omega^4\rangle$ are listed in Table III. From the latter we see that

TABLE III. Comparison of the zeroth and second moments of $S(q,\omega)$ from the MD runs with the earlier Monte Carlo structure factors[1] and with the exact value of the second moment. At small Γ the moments for large q do not reflect the accuracy of the MD results since part of the high-frequency tail of $S(q,\omega)$ was not calculated. Similarly at high Γ and small q the MD results lack sufficient resolution for an accurate calculation of the moments. $I(q)$ is defined below Eq. (3.13).

Γ	q	$\langle\omega^0\rangle$	$S(q)_{\text{M.C.}}$	$\langle\omega^2\rangle$	$q^2/3\Gamma$	$I(q)$
0.993	0.619	0.112	0.118	0.144	0.129	0.0094
	0.875	0.188	0.216	0.241	0.257	0.0182
	1.072	0.296	0.300	0.405	0.386	0.0266
	1.383	0.444	0.433	0.586	0.643	0.0422
	1.856	0.602	0.612	0.979	1.157	0.689
	2.315	0.702	0.739	1.084	3.213	0.0967
	3.094	0.680	0.876	1.183	12.72	0.1420
	6.156		0.994			0.260
9.7	0.619	0.0107	0.0132	0.010	0.0132	0.0135
	0.875	0.0266	0.0273	0.0245	0.0263	0.266
	1.383	0.0765	0.0756	0.0651	0.0659	0.0643
	1.856	0.165	0.155	0.121	0.119	0.111
	2.315	0.258	0.283	0.170	0.184	0.162
	3.094	0.647	0.640	0.313	0.329	0.251
	6.187	0.984	1.004	1.078	1.317	0.341
110.4	0.619	0.000 38	0.001 22	0.000 35	0.001 16	0.0151
	0.875	0.001 25	0.002 56	0.0011	0.002 31	0.0298
	1.383	0.007 24	0.007 58	0.0054	0.005 78	0.0727
	1.856	0.0185	0.0173	0.011	0.0104	0.126
	2.315	0.0353	0.0369	0.015	0.0162	0.188
	3.094	0.169	0.170	0.030	0.0289	0.301
	6.187	0.735	0.715	0.118	0.116	0.306
152.4	0.619	0.000 32	0.000 89	0.000 292	0.000 84	0.0152
	0.875	0.002 59	0.001 89	0.002 39	0.000 168	0.0299
	1.383	0.0052	0.005 55	0.004 02	0.004 20	0.0740
	1.856	0.0138	0.0126	0.008 53	0.0075	0.127
	2.315	0.0268	0.0271	0.0113	0.0117	0.189
	3.094	0.119	0.129	0.0203	0.0209	0.303
	6.187	0.632	0.660	0.0778	0.0838	0.3025

the curves can be extrapolated smoothly to $\langle\omega'^6 S\rangle / S(q) = 1$ at $q = 0$, in agreement with the value of the *exact* sixth moment at $q = 0$ (cf. Appendix A). This satisfactory feature of our results raises the possibility that a fair description of $S(q, \omega)$ could be obtained by incorporating the exact values of the sixth moment, thereby avoiding the use of any adjustable parameter. Work along these lines is in progress.

V. TRANSVERSE COLLECTIVE MODES

The MD work of Levesque *et al.*[20] has shown that shear modes can propagate in dense liquids near their triple point, in a manner not unlike the transverse phonon modes in a solid. These modes appear as peaks in the spectrum of the transverse-current correlation function defined by Eq. (3.6). In complete analogy with the longitudinal case we introduce the Fourier-Laplace transform of (3.6),

$$\tilde{C}_t(k, \omega) = \int_0^\infty e^{i\omega t} C_t(k, t)\, dt, \tag{5.1}$$

the real part of which can be "measured" in the course of the MD computations in a manner similar to the computation of $S(k, \omega)$ from Eq. (3.14). The transverse-current spectrum is

$$C_t(k, \omega) = (1/\pi)\tilde{C}_t'(k, \omega). \tag{5.2}$$

According to Eq. (3.8), the corresponding longitudinal-current spectrum is simply related to $S(k, \omega)$ by

$$C_l(k, \omega) = \omega^2 S(k, \omega). \tag{5.3}$$

Introducing again the dimensionless vector $\vec{q} = a\vec{k}$, the first two moments of $C_t(q, \omega)$ are easily shown to be

$$\langle\omega^0 C_t\rangle = \int_{-\infty}^{+\infty} C_t(q, \omega)\, d\omega = \frac{\omega_p^2 q^2}{3\Gamma} = \omega_0^2, \tag{5.4}$$

$$\langle\omega^2 C_t\rangle = \int_{-\infty}^{+\infty} \omega^2 C_t(q, \omega)\, d\omega = \frac{\omega_p^4}{3\Gamma}\left(\frac{q^4}{3\Gamma} + q^4 I(q)\right). \tag{5.5}$$

On combining the results of (3.13) and (5.5), and remembering (5.3), we immediately obtain the "sum rule"

$$(\langle\omega^2 C_l\rangle + 2\langle\omega^2 C_t\rangle)/\omega_0^2 = \omega_p^2(1 + 5q^2/3\Gamma), \tag{5.6}$$

which is valid for all values of q.

In the limit of large Γ the sum rule (5.6) resembles the well-known Kohn sum rule for the harmonic Wigner lattice (cf. II). At large Γ the dispersion curve for the longitudinal ("plasmon") excitations bears a strong resemblance to the longitudinal phonon branch in the solid, as illustrated in Fig. 8 for the case $\Gamma = 152.4$. It is therefore reasonable to anticipate the appearance of relatively well-defined transverse modes in the fluid OCP in order to saturate the sum rule (5.6).

We have computed $C_t(q, \omega)$ for $\Gamma = 152.4$ and six q values identical to those used for $S(q, \omega)$ except that $q = 2.315$ is excluded. The results are plotted in Figs. 12 and 13. Figure 12 shows spectra for the three lowest q values, and the results for the three largest wave vectors are given in Fig. 13. Whereas the spectra at lower q reduce to rather well-defined single low-frequency peaks, in qualitative agreement with the findings of Levesque *et al.*[20] for the Lennard-Jones fluid, the high-q spectra show a rather unusual structure, as they split into *two* peaks, of which the second corresponds to relatively high frequencies. This is very clear for $q = 3.094$ and $q = 6.156$, but for $q = 1.856$ the rather large statistical errors on $C_t(q, \omega)$ (of the order of 10% even after a MD run of 10^5 time steps!) make it impossible to draw any conclusion concerning the existence of the small secondary peak.

We have analyzed the data on $C_t(q, \omega)$ at the four

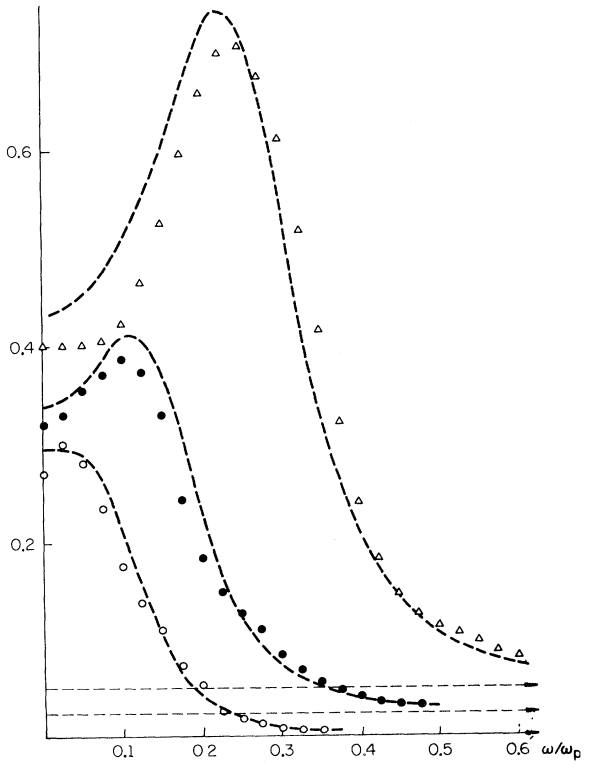

FIG. 12. Spectrum of transverse currents $C_t(q, \omega)$ as a function of ω/ω_p, at $\Gamma = 152.4$ and (from bottom to top of figure) $q = 0.619$, 0.875, and 1.384; triangles: MD results; dashed lines: memory-function fits based on Eq. (5.8).

lowest q values, using again the generalized-hydrodynamics formalism of Kadanoff and Martin.[17] We begin by writing $\tilde{C}_t(q,\omega)$ in the form

$$\tilde{C}_t(q,\omega) = \omega_0^2/[-i\omega + \omega_1^2 \tilde{n}_t(q,\omega)], \tag{5.7}$$

where

$$\omega_1^2 = \langle \omega^2 C_t \rangle / \omega_0^2 = q^2/3\Gamma + I(q)$$

and

$$\tilde{n}_t(q,\omega) = \int_0^\infty e^{i\omega t} n_t(q,t)\, dt.$$

The function $n_t(q,t)$ is the usual memory function.

Proceeding in the manner of Levesque *et al.*[20] we choose a simple exponential form for the memory function, thereby introducing a single unknown relaxation time $\tau(q)$ to account for the short-time collisional processes:

$$n_t(q,t) = e^{-t/\tau(q)}.$$

The corresponding form for $C_t(q,\omega)$ is then

$$C_t(q,\omega) = \frac{\omega_p \tau(q)}{3\pi\Gamma} \frac{\omega_1^2 q^2}{\omega^2 + \tau^2(q)(\omega_1^2 - \omega^2)^2}. \tag{5.8}$$

Equation (5.8) satisfies the moments sum rules (5.4) and (5.5) exactly.

This form of $C_t(q,\omega)$, with $\tau(q)$ as an adjustable parameter, was used in a least-squares fit of our computed $C_t(q,\omega)$. The results for the three lowest q values are shown in Fig. 12. It is clear that the approximation (5.8) can produce only a single peak, and for that reason the high-q fits are very poor and not shown in Fig. 13. However, the lower-q fits are fair, considering the large statistical uncertainties on the MD data. From these fits we obtain an estimate of the dimensionless kinematic viscosity η^*, which is related to the coefficient of shear viscosity η through $\eta^* = \eta/\rho m \omega_p a^2$, by taking the hydrodynamic limit[17]

$$\lim_{\omega\to 0}\lim_{q\to 0}[(\omega^2/q^4) C_t(q,\omega)] = \omega_p \eta^*/3\pi\Gamma. \tag{5.9}$$

Application of (5.9) to (5.8) yields

$$\eta^* = \frac{1}{3\Gamma}\tau(q=0)(1 - \tfrac{2}{15} U/Nk_BT), \tag{5.10}$$

where U/N is the excess internal energy per particle, calculated in I. Plotting $\tau(q)$, obtained from the least-squares fits, versus q and extrapolating the curve to $q=0$, we obtain the estimate $\eta^* \approx 0.26$. This result agrees within 10% with an independent estimate obtained by fitting directly the lowest-q MD data to the limiting hydrodynamic result,[21]

$$C_t^h(q,\omega) = (\omega_p \eta^*/3\pi\Gamma) q^4/(\omega^2 + \eta^* q^4), \tag{5.11}$$

where now η^* is treated as an adjustable parameter. Use of this procedure yields the estimate $\eta^* \approx 0.24$.

The high-q data are more difficult to analyze. It is clear that at least two different relaxation times are needed in order to account for the two peaks. This can be achieved by carrying the continued-fraction expansion[22] of $\tilde{C}_t(q,\omega)$ one order further,

$$\tilde{C}_t(q,\omega) = \omega_0^2 \Big/ \left(-i\omega + \frac{\omega_1^2}{-i\omega + \omega_2^2 \tilde{n}_t(q,\omega)}\right), \tag{5.12}$$

where ω_2^2 is related to the fourth moment of $C_t(q,\omega)$, The spectrum corresponding to (5.12) is

$$C_t(q,\omega) = \frac{\omega_0^2 \tau(q) \omega_1^2 \omega_2^2}{\pi} \times \frac{1}{(\omega^2 - \omega_1^2)^2 + \omega^2 \tau(q)^2 [\omega^2 - (\omega_1^2 + \omega_2^2)]^2}, \tag{5.13}$$

which satisfies the zeroth-, second-, and fourth-moment sum rules exactly, and can, in principle, exhibit two peaks. Using $\tau(q)$ and the unknown ω_2 as variable parameters, the low-q fits are improved, especially at the higher frequencies. However, the discrepancies remain very large at the two highest q values, which seems to indicate that

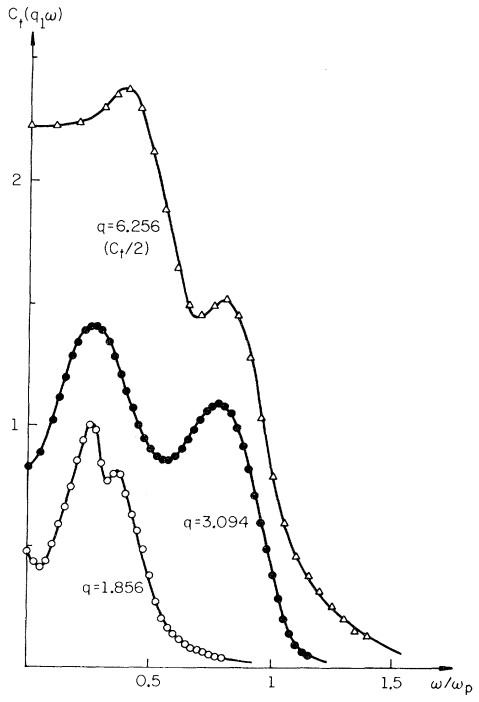

FIG. 13. $C_t(q,\omega)$ as a function of ω/ω_p at $\Gamma = 152.4$ for (reading from bottom to top of figure) $q = 1.856$, 3.094, 6.156. Note that for the highest q value C_t has been divided by 2 for graphical convenience.

a single-exponential form for $n(q,t)$ is insufficient to account for the high-q spectra. A similar conclusion has been reached by Levesque *et al.*[20] in the case of a Lennard-Jones system. A more complete and unified analysis of the longitudinal- and transverse-current correlation functions is at present under way and will be published separately.

VI. CONCLUSIONS

We have carried out extensive MD computations of time-dependent correlation functions for a classical one-component plasma over a very wide range of thermodynamic states between $\Gamma \approx 1$ and $\Gamma \approx 152$ in an effort to understand the single-particle and collective motions in dense plasmas. Our basic conclusion is that *both* types of motions are dominated by the plasma oscillations and the coupling between these and the single-particle modes. This is already very apparent in the behavior of the velocity autocorrelation functions and becomes even more obvious from inspection of the longitudinal density (and charge) fluctuation spectra. Perhaps the most important result of our computations is the evidence of a *qualitative* change in the dispersion curve for the charge fluctuations: between $\Gamma = 1$ and $\Gamma = 10$ the dispersion changes from *positive* (or Vlasov-like) to *negative* (or crystal-like). The simple moments analysis of Sec. III suggests that the change takes place around $\Gamma = 3$, a figure which represents only 2% of the value of Γ at melting (~155). The question naturally arises as to whether one could find experimental evidence for negative dispersion. The usual laboratory plasmas correspond to values of Γ several orders of magnitude below $\Gamma = 3$, and fall into a range where the Vlasov dispersion relation (3.20) is valid. On the other hand, recent experiments on the much more dense solid-state electronic plasmas seem to indicate negative dispersion,[23] though it must be kept in mind that a direct comparison with our results is not possible because of the dominant quantum nature of the electronic plasmas. Negative dispersion in classical systems is, however, not unknown. Recent MD "experiments" on liquid ionic salts (i.e., two-component plasmas with hard cores) has shown that in such system the optic modes exhibit even a stronger negative dispersion[24] than that observed in the OCP.

Another striking result of our computations is the extremely rapid variation in shape of the dynamical structure factor over a relatively small range of the wave number q. For $\Gamma = 10$, 110 and 152, $S(q,\omega)$ for $q = 2.3$ still exhibits a well-defined peak not far from the plasma frequency; at $q = 3.1$, however, the peak has completely vanished. This feature is rather well reproduced by the simple damping-function analysis introduced in Sec. IV.

The present analysis of the spectrum of the transverse-current correlation is less satisfactory, especially for large wave vectors. Our analysis has been hampered by two circumstances. First, we had no prior knowledge of the value of the coefficient of shear viscosity. In principle we could have obtained a direct estimate of η by using the Kubo formula, as was done by Levesque *et al.*[20] for the Lennard-Jones fluid. However, our method of implementing the Ewald method for calculating the total force acting on each particle does not allow a separate calculation of the *pair* forces, hence we were unable to compute the Kubo current appropriate to the shear viscosity. Second, the computer limitations were such that we were able to study only six values of q. Consequently there is a gap between $q = 2$ and $q = 3$ in the range of wave vectors which we investigated, which unfortunately coincides with the appearance of the high-frequency second peak in $C_t(q,\omega)$. It is interesting to note that the appearance of the second peak seems to coincide with the abrupt disappearance of the plasmon peak in $S(q,\omega)$.

Finally, as a by-product of our correlation-function computations, we have obtained numerical values for two transport coefficients of the OCP, the reduced diffusion constant D^* and the reduced coefficient of shear viscosity η^*. To give some feeling for the orders of magnitude of these coefficients we convert them into absolute units in two physical situations. Under normal white-dwarf conditions (10^6 gm cm^{-3}, 10^7 K, and $\Gamma = 5.6$, if we assume a pure helium composition), we find that $D \simeq 2 \times 10^{-3}$ cm^2 sec^{-1}. If we now suppose that the white dwarf is cooled down to a temperature of only 360 000 K (corresponding to $\Gamma = 152$, i.e., close to crystallization), D drops to a value of 3×10^{-3} cm^2 sec^{-1}, which is of the same order of magnitude as the diffusion constant for a simple liquid (e.g., argon) near its triple point. At the same time $\eta = 1.86 \times 10^3$ P, which is *six* orders of magnitude above the corresponding value for liquid argon at the triple point. Thus a super-dense plasma appears as an extremely viscous fluid in which single particles nonetheless diffuse normally.

APPENDIX A

We give here the expressions for the sixth moment of $S(k,\omega)$ [which is the *fourth* moment of $C_1(k,\omega)$], denoted by $\langle\omega^4\rangle_1$, and the fourth moment of $C_t(k,\omega)$, denoted by $\langle\omega^4\rangle_t$. These are calculated

in the standard way from the sixth or, respectively, the fourth time derivative of the corresponding correlation function (3.3) or (3.6), taken at $t=0$, using the equations of motion. Care must be taken to take proper account of the uniform background contribution and to group the various terms so that convergent integrals appear in the final expressions. For these two reasons our expressions differ from the usual formulas which are valid only for short-range potentials.[25] We find

$$\langle \omega^6 S\rangle \equiv \langle \omega^4\rangle_1 = 15\omega_0^6 + 5\omega_0^4\omega_p^2 + \omega_0^2\omega_p^4 + 12\omega_0^4\omega_p^2 \int_0^\infty \frac{g(r)}{r}\left(\frac{45\sin kr}{(kr)^5} - \frac{45\cos kr}{(kr)^4} - \frac{18\sin kr}{(kr)^3} + \frac{3\cos kr}{(kr)^2}\right)dr$$

$$+ \omega_0^2\omega_p^4\left[\frac{4a^3}{3}\int_0^\infty \frac{g(r)}{r^4}\left(1 - \frac{2\sin kr}{kr} - \frac{3\cos kr}{(kr)^2} + \frac{3\sin kr}{(kr)^3}\right)dr\right.$$

$$+ \frac{4}{3}\int_0^\infty \frac{g(r)-1}{r}\left(\frac{3\sin kr}{(kr)^3} - \frac{3\cos kr}{(kr)^2} - \frac{\sin kr}{kr}\right)dr$$

$$\left. + \frac{1}{(4\pi)^2}\int d^3r \int d^3r' [g_3(\vec{r},\vec{r}') - 1][\nabla_r^z \nabla_r^\alpha \phi(r)][\nabla_{r'}^z \nabla_{r'}^\alpha \phi(r')][e^{ik(z-z')} - 2e^{ikz}]\right], \tag{A1}$$

where $\omega_0^2 = k_B T k^2/m$, $g_3(\vec{r},\vec{r}')$ is the triplet distribution function, $\phi(r) = 1/r$, and $\alpha = x, y, z$. Similarly, we find for $\langle \omega^4\rangle_t$,

$$\langle \omega^4\rangle_t = 3\omega_0^6 + \frac{7}{3}\omega_0^4\omega_p^2 - 2\omega_0^4\omega_p^2 \int_0^\infty \frac{g(r)}{r}\left(\frac{9\cos kr}{(kr)^2} - \frac{54\sin kr}{(kr)^3} - \frac{135\cos kr}{(kr)^4} + \frac{135\sin kr}{(kr)^5}\right)dr$$

$$+ \omega_0^2\omega_p^4\left[\frac{2}{3}\int_0^\infty \frac{[g(r)-1]}{r}\left(\frac{\sin kr}{kr} + \frac{3\cos kr}{(kr)^2} - \frac{3\sin kr}{(kr)^3}\right)dr\right.$$

$$+ \frac{2}{3}a^3\int_0^\infty \frac{g(r)}{r^4}\left(2 - \frac{\sin kr}{kr} + \frac{3\cos kr}{(kr)^2} - \frac{3\sin kr}{(kr)^3}\right)dr$$

$$\left. + \frac{1}{(4\pi)^2}\int d^3r \int d^3r' [g_3(\vec{r},\vec{r}') - 1][\nabla_r^x \nabla_r^\alpha \phi(r)][\nabla_{r'}^x \nabla_{r'}^\alpha \phi(r')][e^{ik(z-z')} - 2e^{ikz}]\right]. \tag{A2}$$

Note that as $k \to 0$ the normalized moments $\langle \omega^4\rangle_1/\omega_0^2$ and $\langle \omega^4\rangle_t/\omega_0^2$ show the expected behavior, tending, respectively, towards ω_p^4 and zero.

APPENDIX B

We recall here the argument leading to the long-wavelength δ-function form for the OCP dynamic structure factor. A similar result holds also in the quantum case.[26]

The result depends on the first two sum rules for $S(q,\omega)$ [Eqs. (3.11) and (3.12) in the text, where the wavelength is in units of the ion-sphere radius],

$$\int_{-\infty}^{\infty} S(q,\omega)\,d\omega = S(q), \tag{B1}$$

$$\int_{-\infty}^{\infty} \omega^2 S(q,\omega)\,d\omega = \frac{\omega_p^2 q^2}{3\Gamma}, \tag{B2}$$

and the long-wavelength form for the structure factor [Eq. (3.17) in the text]

$$S(q) = q^2/3\Gamma + O(q^4). \tag{B3}$$

Using (B3) and (B2) gives

$$\int_{-\infty}^{\infty} \omega^2 S(q\omega)\,d\omega = \omega_p^2 S(q) + O(q^4)$$

$$= \int_{-\infty}^{\infty} \omega_p^2 S(q\omega)\,d\omega + O(q^4), \tag{B4}$$

where (B1) was used for the last equality. Rewriting this we have

$$\int_{-\infty}^{\infty} S(q\omega)(\omega^2 - \omega_p^2)\,d\omega = O(q^4), \tag{B5}$$

or

$$\int_{-\infty}^{\infty} \frac{S(q\omega)}{q^3}(\omega^2 - \omega_p^2)\,d\omega = O(q). \tag{B6}$$

Taking $q \to 0$, the right-hand side goes to zero. Since $S(q,\omega)$ is everywhere positive and must have a portion of finite weight going as q^2 [from (B1) and (B3)] (B6) can be satisfied in the small-q limit only if $S(q\omega)$ is nonzero only for $\omega = \omega_p$. (B1),

together with the symmetry of $S(q\omega)$ in the classical case, gives

$$\lim_{q\to 0} S(q\omega) = \tfrac{1}{2} S(q)[\delta(\omega - \omega_p) + \delta(\omega + \omega_p)]. \quad \text{(B7)}$$

In the case of short-range potentials the sum rules (B1) and (B2) hold; however, the completely different behavior of $S(k)$ for small k does not permit the argument made here, and, of course, the long-wavelength behavior of $S(k\omega)$ in these systems is entirely different from that of the OCP.

---

*Laboratoire associé au Centre National de la Recherche Scientifique.

†IBM Postdoctoral Fellow; supported in part by the National Science Foundation Grant GH 33634.

[1]J.-P. Hansen, Phys. Rev. A 8, 3096 (1973).

[2]E. L. Pollock and J.-P. Hansen, Phys. Rev. A 8, 3110 (1973).

[3]N. Metropolis, A. W. Rosenbluth, M. N. Rosenbluth, A. M. Teller, and E. Teller, J. Chem. Phys. 21, 1087 (1953).

[4]J.-P. Hansen, E. L. Pollock, and I. R. McDonald, Phys. Rev. Lett. 32, 277 (1974).

[5]L. Verlet, Phys. Rev. 159, 98 (1967).

[6]S. G. Brush, H. L. Sahlin, and E. Teller, J. Chem. Phys. 45, 2102 (1966).

[7]D. Levesque and L. Verlet, Phys. Rev. A 2, 2514 (1970).

[8]P. G. de Gennes, Physica (Utr.) 25, 825 (1959).

[9]N. G. Van Kampen and B. U. Felderhof, *Theoretical Methods in Plasma Physics* (North-Holland, Amsterdam, 1967), Chap. XI.

[10]R. P. Feynman, Phys. Rev. 94, 262 (1954).

[11]F. H. Stillinger and R. Lovett, J. Chem. Phys. 49, 1991 (1968).

[12]J. F. Springer, M. A. Pokrant, and F. A. Stevens, J. Chem. Phys. 58, 4863 (1973).

[13]M. S. Abramo and M. P. Tosi, Nuovo Cimento (to be published).

[14]A. A. Kugler, J. Stat. Phys. 8, 107 (1973).

[15]M. Nelkin and S. Ranganathan, Phys. Rev. 164, 222 (1967).

[16]J. W. Dufty (private communication).

[17]L. P. Kadanoff and P. C. Martin, Ann. Phys. (N. Y.) 24, 419 (1963); P. C. Martin and S. Yip, Phys. Rev. 170, 151 (1968).

[18]R. Kubo, Rep. Prog. Phys. 29, 255 (1965).

[19]K. Kim, Ph.D. thesis (Cornell University, 1971) (unpublished).

[20]D. Levesque, L. Verlet, and J. Kurkijarvi, Phys. Rev. A 7, 1690 (1973).

[21]P. Schofield, in *Physics of Simple Liquids*, edited by H. N. V. Temperley, J. S. Rowlinson, and G. S. Rushbrooke (North-Holland, Amsterdam, 1968).

[22]J. Mori, Prog. Theor. Phys. 34, 399 (1965).

[23]P. M. Platzman and P. Eisenberger, Phys. Rev. Lett. 33, 152 (1974).

[24]A. Rahman (private communication); J.-P. Hansen and I. R. McDonald (unpublished).

[25]D. Forster, P. C. Martin, and S. Yip, Phys. Rev. 170, 155 (1968).

[26]D. Pines and P. Nozieres, *The Theory of Quantum Liquids* (Benjamin, New York, 1966), p. 220.